bioRχiv
THE PREPRINT SERVER FOR BIOLOGY

ARTICLE PREPRINT

Combined modulation of SHH and FGF signaling is crucial for maintenance of the neocortical progenitor specification program

Odessa R. Yabut[1, #], Hui-Xuan Ng[1, #], Keejung Yoon[1, 2], Hector G. Gomez[1], Jessica C. Arela[1], and Samuel J. Pleasure[1, 3, *]

ABSTRACT

Neuronal progenitors in the developing forebrain undergo dynamic competence states. This process ensures timely generation of specific excitatory and inhibitory neuronal subtypes from distinct neurogenic niches of the dorsal and ventral forebrain, respectively. Here we show evidence of progenitor plasticity when Sonic hedgehog (SHH) signaling is left unmodulated in the embryonic neocortex of the dorsal forebrain. At early stages of corticogenesis, loss of Suppressor of Fused (Sufu), a potent intracellular inhibitor of SHH signaling, can alter the transcriptomic landscape of neocortical progenitors. Ectopic activation of SHH signaling in neocortical progenitors increase expression of Fibroblast Growth Factor 15 (FGF15), consequently activating FGF and MAPK signaling and inducing expression of genes characteristic of ventral forebrain progenitors. Ultimately, neocortical progenitors differentiate into misspecified excitatory neurons or surprisingly, inhibitory neurons. Thus, our studies underscore the importance of modulating extrinsic niche signals in early corticogenesis to maintain the competency and specification program of neocortical progenitors.

INTRODUCTION

The adult mammalian neocortex is composed of an intricate network of diverse excitatory and inhibitory neurons derived from distinct progenitor domains of the embryonic forebrain. Excitatory neurons originate from the ventricular and subventricular zones (VZ/SVZ) of the embryonic neocortex, while inhibitory neurons (interneurons) originate from the ganglionic eminences (GE). During corticogenesis, radial glial cells (RGC) populating the VZ/SVZ sequentially generate deep-layer excitatory neurons, followed by upper-layer excitatory neurons via intermediate progenitor (IPC) or outer radial glial (oRG) cells (Beattie and Hippenmeyer, 2017). Similarly, interneurons are sequentially generated in a layer-specific manner by RGCs in the GE and subsequently undergo a long tangential migration into specific neocortical layers (Lim et al., 2018). This process must be tightly regulated since an imbalance between excitatory and inhibitory activity underlie a number of neurological and neuropsychiatric disorders (Sohal and Rubenstein, 2019).

A combination of intrinsic and extrinsic cues guides and maintains the specification program of neocortical progenitors throughout corticogenesis to generate neuronal diversity. But how these cues are integrated in neocortical progenitors to produce distinct neuronal subtypes in a temporal manner is still largely unclear. Our previous work identified fundamental mechanisms at early stages of corticogenesis ensuring proper specification of neocortical progenitors into distinct excitatory neuronal lineages, through modulation of Sonic hedgehog (SHH) signalling pathway (Yabut et al., 2015). SHH signalling is triggered upon binding of SHH

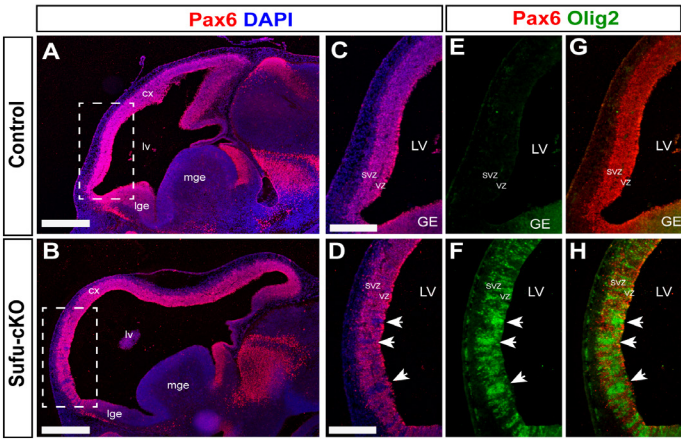

Figure 1. Specification defects are evident in discrete regions of the neocortex of the E12.5 mice lacking Sufu.
A-B, Immunostaining using dorsal forebrain progenitor marker, Pax6, and DAPI counterstain, show high Pax6 expression in the dorsal forebrain (cx) compared to the lateral (LGE) or medial (MGE) ganglionic eminence in both the E12.5 control and Sufu-cKO embryonic forebrains. Scale bar = 500 μm.
C-D, Higher magnification of boxed regions in A and B show low or absent Pax6 expression in specific areas of the rostral neocortex of Sufu-cKO forebrains (D, arrows) but not in controls (C). Sections are counterstained with DAPI. Scale bar = 250 μm.
E-H, Double immunostaining with Pax6 and Olig2, a ventral forebrain progenitor marker, show ectopic expression of Olig2 in areas where Pax6 is missing in the Sufu-cKO neocortex (F, H, arrows), whereas Olig2 is not expressed in this region in the control neocortex (E, G). Scale bar = 250 μm.

1. Department of Neurology, University of California, San Francisco, California, USA. 2. College of Biotechnology and Bioengineering, Sungkyunkwan University, Suwon, Gyeonggi-do 440-746, Republic of Korea 3. 3Programs in Neuroscience and Developmental Biology, Eli and Edythe Broad Center of Regeneration Medicine and Stem Cell Research, University of California San Francisco, California, USA
[#]These authors contributed equally to this work. *Corresponding Author: sam.pleasure@ucsf.edu

ligands to the transmembrane receptor Patched 1 (Ptch1), which relieves its inhibition of another transmembrane protein, Smoothened (Smo). Consequently, Smo initiates a cascade of intracellular events promoting the nuclear translocation of Gli, a family transcription factors, to activate SHH target gene expression. However, intracellular checkpoints are present to modulate SHH signalling. In the developing neocortex, Suppressor of Fused (Sufu), a potent inhibitor of SHH signalling, is highly expressed in neocortical progenitors to modulate SHH signals to ensure the production of molecularly distinct upper and deep layer excitatory neurons (Yabut et al., 2015). Sufu exerted this effect by ensuring the stable formation of Gli transcription factors, the downstream effectors of SHH signalling. Specifically, loss of Sufu resulted in the degradation of the repressor form of Gli3 (Gli3R), the predominant Gli protein in the developing neocortex (Fotaki et al., 2006; Palma and Ruiz i Altaba, 2004; Wang et al., 2011; Wilson et al., 2012) leading to the production of misspecified neocortical progenitors by mid-corticogenesis. However, little is known on the identity of downstream molecular targets of SHH signalling or Gli3 in neocortical progenitors, and how deregulation of these targets due to uncontrolled SHH signalling might affect neocortical progenitor fates.

Here we show that endogenous levels of SHH, in the absence of Sufu, can sufficiently increase SHH signalling activity in neocortical progenitors resulting in drastic changes in the transcriptomic landscape of the VZ/SVZ at early stages of corticogenesis. In accordance to our previous findings, ventral forebrain progenitor gene transcripts are already ectopically expressed in neocortical progenitors in the embryonic (E) 12.5 neocortex mice lacking Sufu. Additionally, we find that activation of Fibroblast Growth Factor (FGF) signalling, via the upregulated gene expression of FGF15, leads to the misspecification of progenitors, particularly affecting the production of IPCs. Surprisingly, these changes not only produced excitatory neurons with mixed identities, but also neocortical progenitor-derived interneurons. These novel findings reveal that uncontrolled SHH signalling can re-define progenitor competency in the embryonic neocortex. Further, this underscores the importance of intrinsic cellular responses, via modulatory proteins such as Sufu, to temporally restrain extrinsic niche signals that can influence progenitor identity and fate.

RESULTS

Specification defects are evident in discrete regions of the neocortex of E12.5 embryonic mice lacking Sufu.

The role of SHH signaling in neocortical neuron specification is critical prior to E13.5, a timepoint at which superficial projection neurons are just beginning to differentiate. Analysis of mice in which Sufu is conditionally deleted at E10.5 in neocortical progenitors using the Emx1-Cre driver (Emx1-cre/+;Sufu-fl/fl or Sufu-cKO), revealed that modulating SHH signaling is critical to properly specify distinct superficial and deep layer projection neurons, after dorsoventral patterning of the forebrain (Yabut et al., 2015). Indeed, Pax6, which is highly expressed in neocortical radial glial (RG) progenitors (Ypsilanti and Rubenstein, 2016) is detected exclusively in dorsal forebrain regions of the E12.5 Sufu-cKO brain and not in the ganglionic eminence (GE) in both control and Sufu-cKO embryos (**Figure 1A-B**). However, Pax6 expression was noticeably intermittent in the more anterior regions of the E12.5 Sufu-cKO neo-

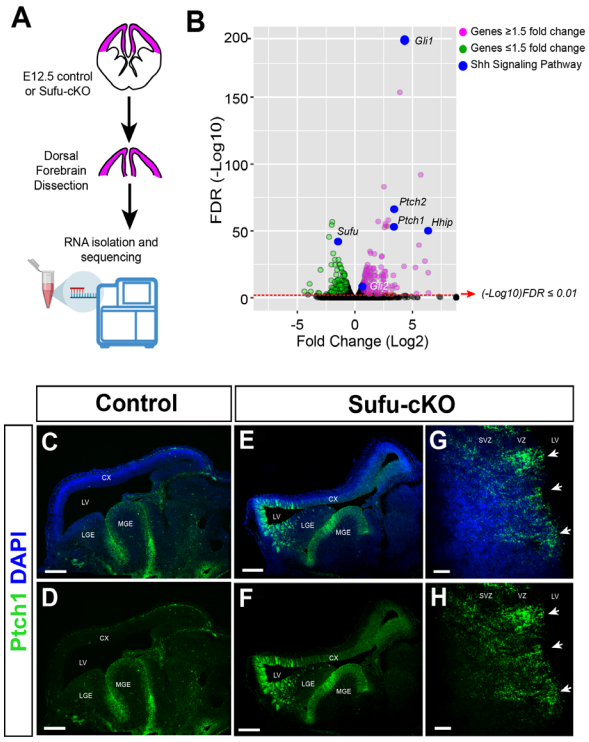

Figure 2. Upregulated expression of SHH signaling gene targets in neocortical progenitors of the E12.5 Sufu-cKO dorsal forebrain.

A, Schematic showing dorsal forebrain areas (pink) dissected from control and mutant E12.5 mice for RNA-Seq analysis. **B,** Volcano plot of RNA-Seq data set highlighting differentially expressed genes with adjusted p value < 0.01 (FDR (-Log10)) and Fold Change (Log2) ≥ 1.5 (red circles) or Fold Change (Log2) ≤ 1.5 (green circles), and genes in the SHH signaling pathway (blue circles), between the E12.5 dorsal forebrain of controls and Sufu-cKO E12.5 embryos.

C-F, RNAscope in situ hybridization (ISH) on sagittal brain sections using probes for Patched 1 (Ptch1) validates upregulation of Ptch1 RNA expression in the E12.5 Sufu-cKO dorsal forebrain (E, F) whereas Ptch1 RNA expression is only detected in the MGE of controls (C, D).Scale bar = 500 μm.

G-H, Higher magnification of rostral neocortex of E12.5 Sufu-cKO dorsal forebrain showing Ptch1 RNA expression is preferentially higher along the ventricular zone (VZ) and subventricular zone (SVZ) where neocortical progenitors are localized. Ptch1 expression also appear in columns, radiating inward from the apical VZ (arrows). Sections in G is counterstained with DAPI. Scale bar = 25 μm.

cortex (boxed region in Figures 1A-B). Areas lacking Pax6 exhibited a columnar distribution hinting at anomalous clones of RGCs (**Figure 1C-D**). We found that these progenitors are improperly specified since we detected ectopic expression of the ventral forebrain progenitor marker, Olig2. Specifically, Olig2 expression was present in areas where Pax6 expression was absent in the E12.5 Sufu-cKO neocortex (arrows in **Figure 1D, 1F, 1H**), whereas Olig2 is completely absent in the neocortex of control mice (**Figure 1E**). Therefore, despite having properly formed dorsal forebrain domains, the specification programs of neocortical RGCs are already aberrant in the E12.5 Sufu-cKO neocortex.

Upregulated expression of SHH signaling targets in Sufu mutant neocortical progenitors

Ectopic expression of Olig2 indicates altered molecular properties of neocortical progenitors in the E12.5 Sufu-cKO neocortex. To gain further insight into these molecular changes, we isolated total RNA from dissected control and mutant neocortices for transcriptome profiling by RNA-Seq (**Figure 2A**). We confirmed that SHH signaling gene targets such as Gli1, Patched 1 and 2 (Ptch1 and Ptch2), and the Hedgehog-Interacting Protein (Hhip) are specifically upregulated in the E12.5 Sufu-cKO neocortex compared to controls (**Figure 2B**) in accordance with our previous findings (Yabut et al., 2015). We validated these observations by in situ hybridization using probes for Ptch1, which was ectopically expressed throughout the neocortical expanse (**Figure 2E-2F**) in contrast to controls (**Figure 2C-2D**). Levels of Ptch1 expression were confined within the progenitor zones (**Figure 2G-2H**), and were particularly high in rostral neocortical regions. Interestingly, expression of Ptch1 also followed a columnar pattern (**Figure 2G-2H**, arrows) similar to the anomalous expression pattern of OLIG2 (**Figure 1F-1H**). These findings indicated deregulation of SHH signaling in discrete neocortical progeni-

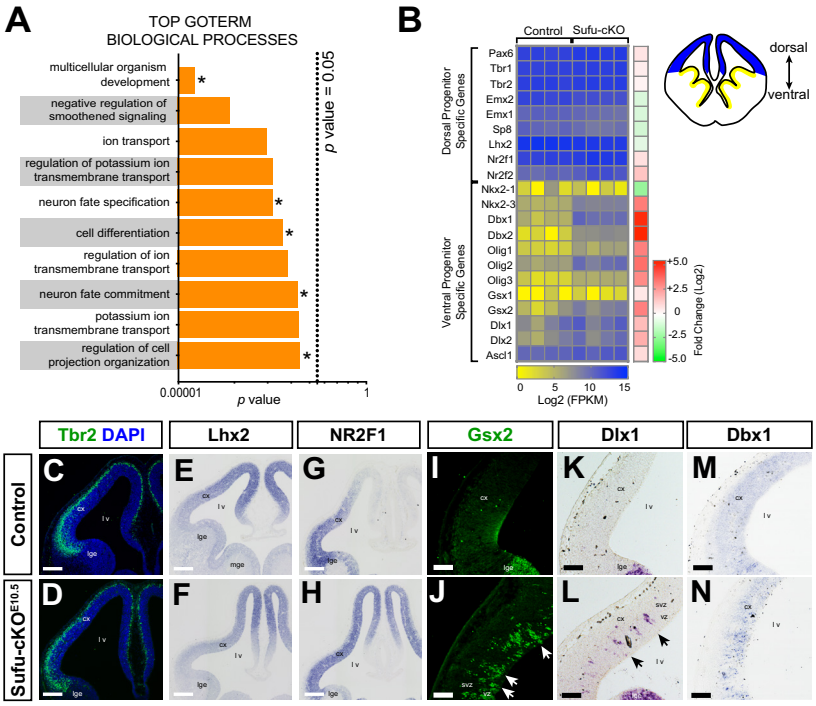

Figure 3. Increased expression of ventral progenitor markers in neocortical progenitors of E12.5 Sufu-cKO embryos.
A, Functional annotation of differentially expressed genes identified by RNA-Seq show top GOTERM Biological Processes (with adjusted p value < 0.05) involve development, specification, differentiation, and fate commitment (asterisks). There is also a notable enrichment in ion transmembrane transport GOTERMs reflecting disrupted electrophysiological properties due to abnormal differentiation of neurons or specific neuronal subtypes.
B, Heat-map of select genes typically expressed by dorsal or ventral progenitors in individual control and Sufu-cKO mice (n=4 mice per genotype). RNA levels (Log2 FPKM scale) reflect mild differences in expression of dorsal progenitor genes (reflected by Fold Change scale), while dramatic differences in expression levels of ventral progenitor genes is observed between controls and Sufu-cKO dorsal forebrain. See also Supplemental Table 1.
C-H, Immunostaining for Tbr2 (C and D, counterstained with DAPI), and ISH for Lhx2 and NR2F1 (E-H) showing genes typically expressed in dorsal forebrain cells remain expressed in the E12.5 neocortex in both control and Sufu-cKO mice. Scale bar = 100 μm.
I-N, Immunostaining for Gsx2 (I, J) and ISH for Dlx1 and Dbx1 show validate the ectopic RNA expression of genes typically expressed by ventral progenitors in the E12.5 Sufu-cKO neocortex (J, L, N) whereas these genes are absent in controls (I, K, M). Gsx2-expressing (Gsx2+) and Dbx1-expressing (Dbx1+) cells largely localized in the VZ and SVZ, while Dlx1 is higher in the SVZ, of the Sufu-cKO neocortex. Some groups of cells expressing Gsx2 and Dlx1 also appeared in columnar arrangement (L and N, arrows). Scale bar = 100 μm.

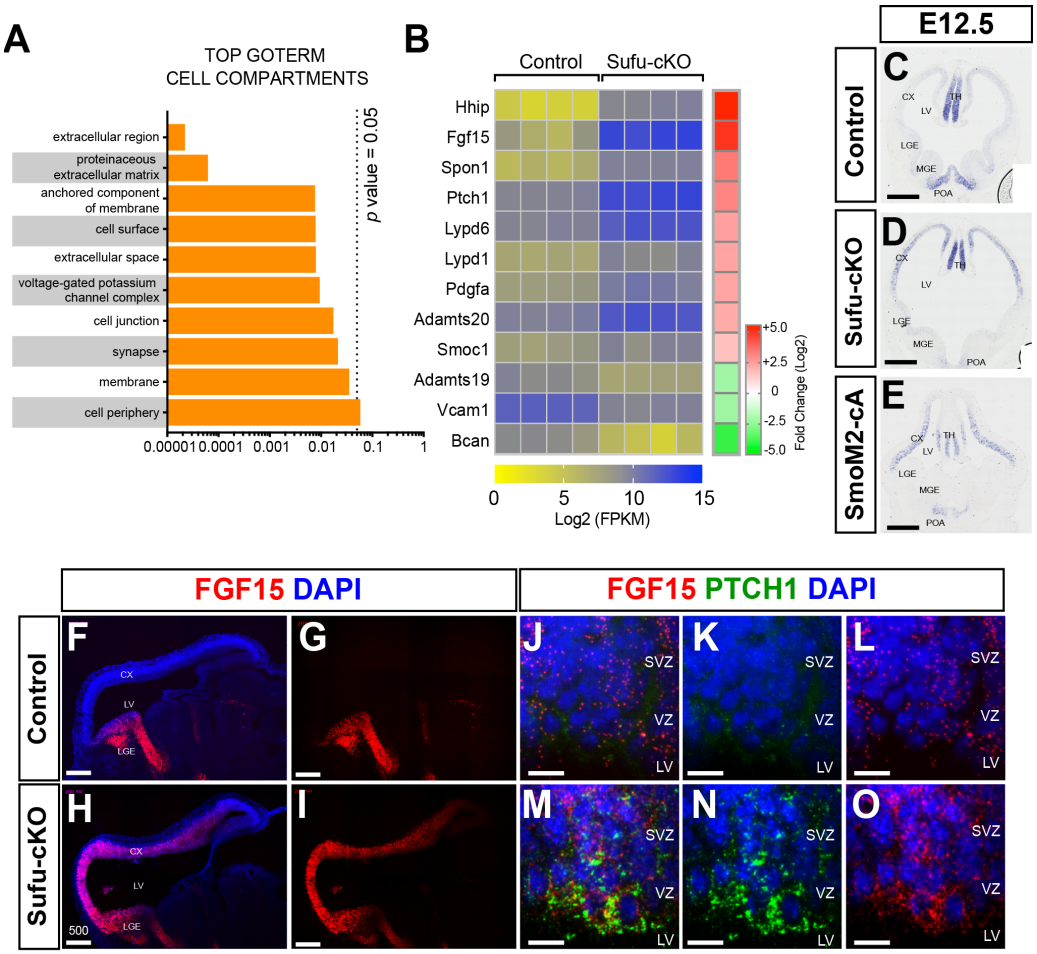

Figure 4. Ectopic activation of SHH signaling drives Fgf15 expression in neocortical progenitors of E12.5 Sufu-cKO embryos.
A, Functional annotation of differentially expressed genes identified by RNA-Seq showing the majority of genes encode proteins that localize to extracellular matrix or cell surface/membrane as the top GOTERMs Cell Compartments (with adjusted p value < 0.05).
B, Heat map of top differentially expressed genes encoding extracellular matrix or cell membrane bound proteins between control and Sufu-cKO mice (n=4 mice per genotype). RNA levels (Log2 FPKM scale) show expression of Fgf15 is significantly upregulated (reflected by Fold Change scale in the E12.5 Sufu-cKO dorsal forebrain. See also Supplemental Table 2.
C-E, ISH for Fgf15 show high levels of Fgf15 expression in the dorsal thalamus (TH) and preoptic area (POA), but low or undetected expression in the neocortex of E12.5 controls (C). In contrast, in addition to the TH and POA, ectopic expression of Fgf15 span along the neocortical wall of E12.5 Sufu-cKO (D) and SmoM2-cA (E) forebrains confirming that activation of SHH signaling and loss of Sufu force Fgf15 expression in the embryonic neocortex. Scale bar = 100 μm.
F-I, RNAscope ISH on sagittal E12.5 brain sections using Fgf15 riboprobes show ventral forebrain expression of Fgf15 in controls (F, G). However, very high levels of Fgf15 is detected in rostral neocortical regions compared to caudal regions of E12.5 Sufu-cKO neocortex (H, I). Sections in F and H are counterstained with DAPI. Scale bar = 500 μm.
J-O, Multiplex RNAscope ISH of Ptch1 and Fgf15 riboprobes on E12.5 brains do not detect Ptch1 expression, while low levels of Fgf15 expression is detected in the VZ and SVZ of the neocortex of controls (J-L). In the E12.5 Sufu-cKO neocortex, high levels of Ptch1 (N) and Fgf15 (O) colocalization is detected in the VZ and SVZ. Sections are counterstained with DAPI. Scale bar = 10 μm.

tor subpopulations, and not differentiated neurons, in the E12.5 neocortex of Sufu-cKO mice.

Altered Molecular Identity of Progenitors in the E12.5 Sufu-cKO Neocortex

Since changes in SHH signaling activity in the neocortex are known to disrupt progenitor fate specification in late-stage corticogenesis (Komada et al., 2008a; Wang et al., 2016), we wondered if the ectopic activation of SHH signaling at E12.5 has initiated a cascade of disruptive differentiation events. Enrichment analyses found over-representation of genes with gene ontology (GO) terms associated with neural development, commitment, specification and differentiation (**Figure 3A**). Further examination of specific gene expression showed relatively mild changes in the expression of genes typical of dorsal forebrain progenitors (**Figure 3B** and **Supplemental Table 1**). Indeed, similar to Pax6 expression in **Figure 1**, other markers for dorsal fore-

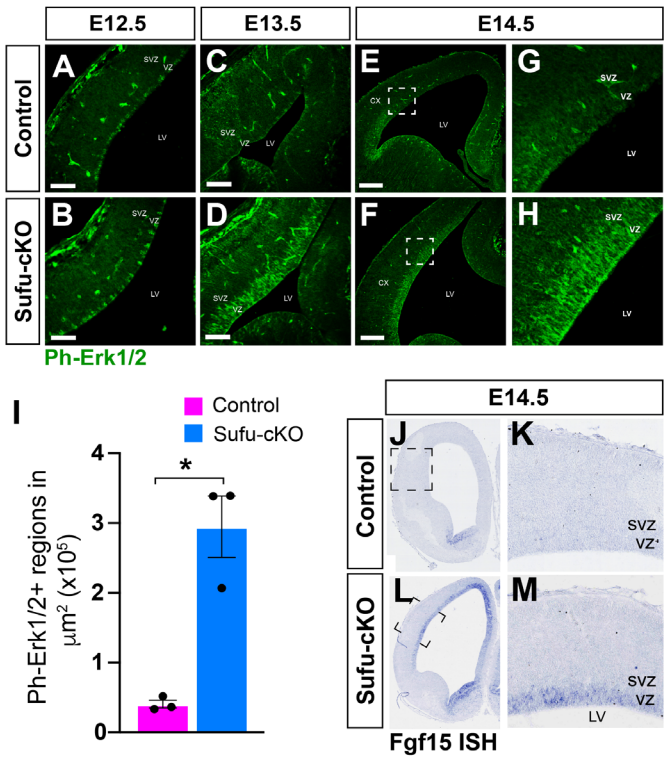

Figure 5. Upregulated FGF15 expression correlates with ectopic activation of MAPK signaling in neocortical progenitor zones.

A-H, Immunostaining against Phosphorylated Erk1/2 (Ph-Erk1/2) was conducted on E12.5, E13.5, and E14.5 control and Sufu-cKO brains to detect for MAPK signaling activation. Ph-Erk1/2-expressing cells (Ph-Erk1/2+) is present in a single cell layer along the apical VZ of E12.5 control and Sufu-cKO neocortex (A, B). This expression pattern remains in the E13.5 control neocortex (C) but not in the Sufu-cKO neocortex where Ph-Erk1/2+ cells expands towards the SVZ (D). At E14.5, Ph-Erk1/2+ cells are present in the VZ/SVZ of the control neocortex with higher expression detected in dorsolateral areas (E, G) whereas Ph-Erk1/2 cells have expanded in more dorsal regions of the Sufu-cKO neocortex (G, H). Scale bar = 100 μm (A, B) and 200 μm (C-F).

I, Bar graph of quantification of Ph-Erk1/2+ regions in the neocortex of E14.5 control and Sufu-cKO mice (n=3 embryos per genotype) showing significant expansion of Ph-Erk1/2+ regions in Sufu-cKO neocortex (p value = 0.0321).

J-M, ISH for Fgf15 show low or undetected levels of Fgf15 in the E14.5 control neocortex (J, K) whereas Fgf15 is ectopically expressed along the progenitor VZ/SVZ regions of the E14.5 Sufu-cKO neocortex (L, M).

brain cells such as Tbr2, Lhx2, and Nr2f1, remained expressed, and may be even expressed at higher levels in the mutant neocortex as observed with Nr2f1 or Nr2f2 (**Figure 3B** and **Supplemental Table 1**). These findings validated the efficiency of the dissection and confirmed that the dorsal identity of neocortical progenitor domains was established in the E12.5 Sufu-cKO neocortex.

Nevertheless, RNA levels for several ventral progenitor genes dramatically increased in the E12.5 Sufu-cKO neocortex compared to controls (**Figure 3B**). These include an increase in Olig2 transcript levels (**Supplemental Table 1**) in agreement with the anatomic observations (**Figure 1E-H**). Moreover, while we previously did not observe a significant increase in Ascl1 protein expression in the E12.5 neocortex (Yabut et al., 2015), we find significantly higher levels of Ascl1 transcript. Additionally, significant upregulation of genes normally expressed in the ganglionic eminence such as Dbx1, Gsx2, and Dlx1/2 (Petryniak et al., 2007) were also present in the neocortex of E12.5 Sufu-cKO mice (**Figure 3B**). We subsequently conducted immunostaining or in situ hybridization experiments to validate the expression of ventral progenitor markers. We found ectopically expressed Gsx2, Dlx1, and Dbx1 the E12.5 neocortex of Sufu-cKO mice. Expression of these genes were detected in the SVZ and VZ regions of the E12.5 Sufu-cKO neocortex and exhibited a columnar pattern (**Figure 3J, 3L, 3N**), whereas these genes were absent in controls (**Figure 3I, 3K, 3M**). These were reminiscent of the expression pattern of OLIG2 or PAX6 (**Figure 1**). Altogether, these findings establish that activation of SHH signaling in early stages of corticogenesis does not disrupt the regionalization of dorsoventral axis but destabilizes the specification program of neocortical RGCs.

Ectopic activation of SHH signaling upregulates FGF15 expression.

To identify the molecular factors mediating the specification defects in the E12.5 Sufu-cKO neocortex, we further analyzed the overall nature of differentially expressed genes from our RNA-Seq data. Interestingly, transcriptomic changes within the E12.5 Sufu-cKO neocortex involved genes encoding proteins with roles in cell-cell communications such as membrane-bound or extracellular matrix proteins (**Figure 4A**). Thus, the molecular make-up of the VZ/SVZ progenitor niche has been significantly altered in response to the ectopic activation of SHH signaling in the E12.5 Sufu-cKO neocortex. Among these is the gene encoding the secreted ligand, Fibroblast Growth Factor 15 (Fgf15) (**Figure 4B**). Fgf15 is a known target of SHH signaling and has been recently shown to be significantly upregulated in the developing cerebellum of mice lacking Sufu (Gimeno and Martinez, 2007; Kim et al., 2018; Komada et al., 2008b). Similarly, in the E12.5 Sufu-cKO neocortex, Fgf15 dramatically increased (+5.72 Log2 Fold Change, p-value < 0.0001). *In situ* hybridization using Fgf15 riboprobes confirmed these findings, with Fgf15 ectopically expressed throughout the neocortical wall of the E12.5 Sufu-cKO mice while Fgf15 expression was relatively low in controls (**Figure 4C-4D**). We also observed upregulation of Fgf15 in embryos in which Smo was constitutively active in neocortical progenitors (Emx1-Cre;SmoM2 or SmoM2-

cA) (Long et al., 2001), confirming the role of activated SHH signaling in inducing FGF15 gene expression (**Figure 4E**). Further, we found that similar to Ptch1 expression (**Figure 2E, 2F**), Fgf15 exhibited higher transcript levels in rostral regions of the neocortex in mutants (**Figure 4F-4G, 4K-4L**). Although we were able to detect low levels of Fgf15 expression in the VZ/SVZ regions of the control neocortex (**Figure 4H-4J**), Fgf15 expression was significantly higher, displayed a columnar pattern, and overlapped with Ptch1-expressing cells (**Figure 4M-4O**). Taken together, these findings suggest that Fgf15 expression in neocortical progenitors in the VZ/SVZ is typically repressed by Gli3R and is relieved from this repression in the absence of Sufu or overactivation of SHH signaling.

Upregulated FGF15 expression correlates with ectopic activation of MAPK signaling in neocortical progenitor zones.

FGF15 preferentially binds to FGF receptor 4 (FGFR4) to activate two intracellular signaling cascades: the Ras/mitogen activated protein kinase (MAPK) and the phosphatidylinositol 3-kinase/AKT pathways (Guillemot and Zimmer, 2011). In the neocortex of Sufu-cKO mice, we found no visible difference in activation of MAPK signaling, as marked by phosphorylated-ERK1/2 (P-ERK1/2+) labeling at E12.5 when compared to controls (**Figure 5A-5B**). However, by E13.5, we observed an increase in P-ERK1/2 labeling in the VZ/SVZ regions (**Figure 5D**), a timepoint at which MAPK signaling activity was largely absent in the neocortex of control mice (**Figure 5C**). By E14.5, MAPK signaling extended throughout more dorsal regions of the Sufu-cKO neocortex, whereas MAPK activity was largely confined in the dorsoventral boundary of the control neocortex (**Figure 5E-5H**). Quantification of P-ERK1/2+ regions in the E14.5 neocortex confirmed these observations and showed a significant increase in Sufu-cKO mice (**Figure 5I**). The increase in P-ERK1/2 labeling in the VZ/SVZ completely overlapped with areas where ectopic expression of FGF15 persisted in the E14.5 Sufu-cKO neocortex but remained undetected in controls (**Figure 5J-5M**) Taken together, these observations indicate that loss of Sufu resulted in the overexpression of FGF15 in the neocortex, subsequently driving the ectopic activation of MAPK signaling in neocortical progenitors.

SHH signaling synergizes with FGF15 signaling to inhibit production of neocortical intermediate progenitors.

Reduction in intermediate progenitors (IP) is a consistent phenotype in the embryonic neocortex of mice with excessive levels of SHH signaling, including in Sufu-cKO mice (Dave et al., 2011; Komada et al., 2008a; Yabut et al., 2015). We therefore investigated whether downregulation of IPs in the neocortex due to ectopic SHH signaling is mediated by FGF15 signaling. To test this, we cultured wildtype forebrain slices from the anterior regions of E12.5 control and Sufu-cKO embryos (**Figure 6A**). Forebrain organotypic cultures maintain the three-dimensional structure of the VZ/SVZ niche, allowing for careful examination of how precisely added compounds affect progenitor behavior over time. As shown in **Figure 6B-6D**, forebrain slices cultured for 2 days in vitro (DIV) maintain their anatomical

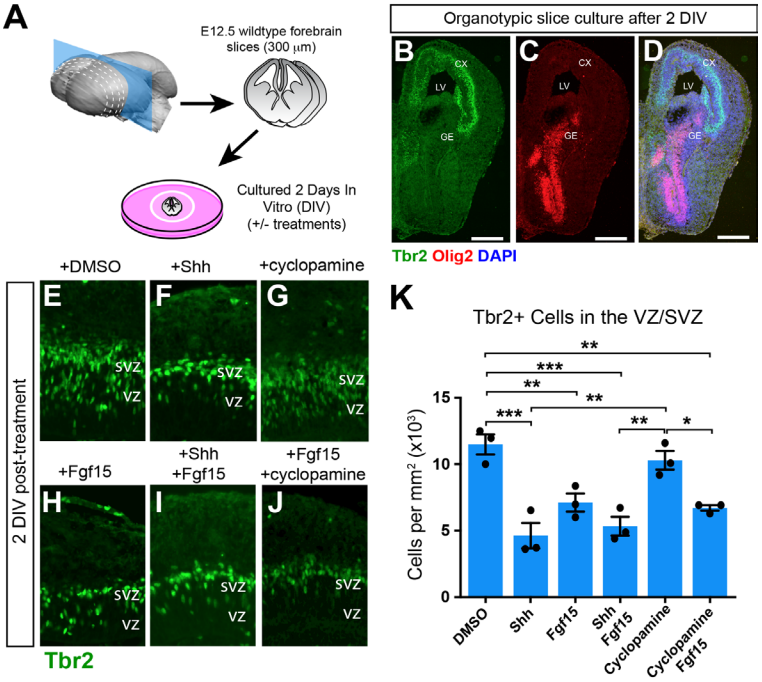

Figure 6. SHH signaling synergizes with FGF15 signaling to inhibit production of neocortical intermediate progenitor cells.
A, Diagram of experimental design for organotypic forebrain slice cultures from wildtype E12.5 brains.
B-D, Immunofluorescence staining for dorsal (Tbr2, green) and ventral (Olig2, red) forebrain markers show exclusive localization of Tbr2 (B) and Olig2 (C) -expressing cells in dorsal and ventral forebrain regions, respectively. Merged images in (D) show no overlap in Tbr2 or Olig2 labeling. Scale bar = 500 μm.
E-K, Immunofluorescence staining with Tbr2, an intermediate progenitor cell (IPC) marker of sectioned organotypic slice cultures fixed after 2 days in vitro (DIV). Slices treated with 200 ng/ml SHH (F) and 100 ng/ml FGF15 (H) show reduced numbers of Tbr2+ IPCs compared to slices treated with DMSO (E) or 5μM Cyclopamine (G). Combined FGF15 and SHH (I) or FGF15 and cyclopamine (J) also show reduced Tbr2+ IPCs. Quantification of Tbr2+ cells per unit area (K) confirm significant differences in Tbr2+ IPCs in SHH and FGF15-treated slice cultures (n = 3 experiments (2-3 slices each experiment) per treatment condition). * = p value ≤ 0.05, ** = p value ≤ 0.03, *** = p value ≤ 0.01.

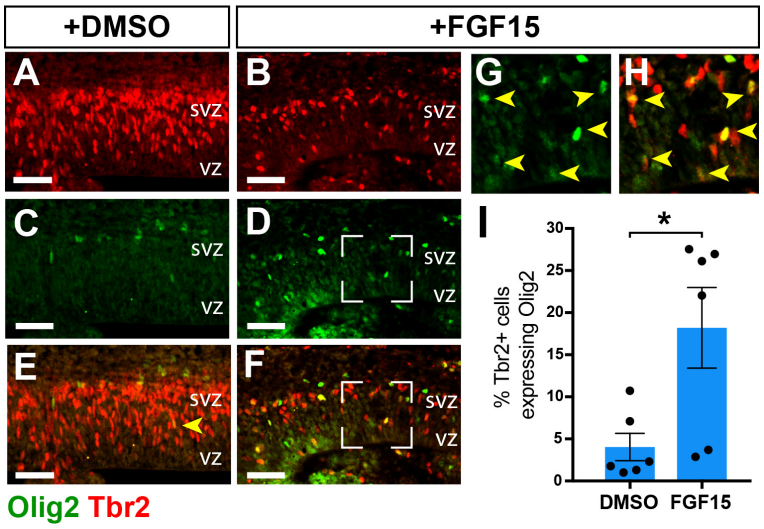

Figure 7. Increasing FGF15 levels alter the specification program of neocortical progenitors.
A-F, Double immunofluorescence staining with IPC marker Tbr2 (red), and the ventral progenitor marker Olig2 (green) on organotypic slice cultures fixed 2 DIV and post-treatment. DMSO-treated slices show an abundance of Tbr2+ IPCs in the SVZ (A) and some Olig2-expressing cells outside of the VZ/SVZ area (B). In contrast, Tbr2+ IPCs in FGF15-treated slices are fewer (B) and more Olig2+ cells are present in the VZ/SVZ (F). Although Tbr2+ cells expressing Olig2 were also sometimes observed in DMSO-treated slices (yellow arrow, C), the amount of double-labeled in FGF15-treated slices were visibly higher in the VZ/SVZ (yellow arrows, G and H). Scale bar = 50 μm.
I, Graph represents the % of Tbr2+ cells colabeled with Olig2 in the VZ/SVZ of DMSO- and FGF15- treated slices (n = 3 experiments (2-3 slices each experiment) per treatment condition). The percentage of Tbr2+ co-expressing Olig2 is ~4-fold in FGF15-treated over control DMSO-treated slices and is significantly higher (* = p value ≤ 0.05).

features with well-preserved dorsal and ventral domains. IPCs typically expressing Tbr2 (Hevner, 2019) were exclusively observed in the dorsal forebrain whereas ventral forebrain progenitors are typically expressing Olig2 (Miyoshi et al., 2007). Predictably, addition of SHH ligands significantly decreased the number of Tbr2+ cells in neocortical slices after 2 DIV when compared to mock-treated controls (**Figure 6E-6F, 6K**). Similarly, Tbr2+ IPs were significantly reduced upon addition of FGF15 alone or with SHH (**Figure 6H-6I, 6K**). Addition of cyclopamine did not alter Tbr2+ IPs in cultured slices (**Figure 6G**). However, combined treatment of cyclopamine and FGF15 significantly reduced the number of Tbr2+ IPs after 2 DIV (**Figure 6J, 6K**). These findings confirmed that increasing levels of FGF15 reduce the number of Tbr2+ IPs, and that this is likely a downstream effect when SHH signaling is ectopically activated in the developing neocortex.

High levels of FGF15 alter the specification program of neocortical progenitors.

Ectopic SHH signaling in the developing neocortex ultimately results in the production of confused progenitors unable to maintain a specified neocortical neural fate (Yabut et al., 2015). The expansive ectopic activation of MAPK signaling, capable of altering neocortical progenitor fate (Wang et al., 2012), in the Sufu-cKO embryonic neocortex (**Figure 5**) is a likely consequence of increasing levels of FGF15. We tested this by adding FGF15 in organotypic forebrain cultures and examined if this alone altered the fate of neocortical progenitors based on Olig2 expression. Indeed, we found that after 2 DIV, the decrease in Tbr2+ IPs correlated with an obvious increase in Olig2+ cells in FGF15-treated slices compared to DMSO-treated controls (**Figure 7A-7D**). Further, low levels of Olig2 expression were detectable in the VZ region, where Olig2 is typically not expressed, and may co-express low levels of Tbr2, indicating that treatment of FGF15 alters the identity of RG progenitors transitioning into IP (**Figure 7G-7H, arrows**). Indeed, many Olig2+ cells in the SVZ also expressed Tbr2 in FGF15-treated slices compared to DMSO-treated controls (**Figure 7E, 7F**). Our quantification confirmed these observations, showing the approximately 4.5-fold increase in misspecified Tbr2+ cortical progenitors in FGF15-treated slices compared to DMSO-treated controls (**Figure 7I**). These findings indicate that excessive levels of FGF15 can sufficiently alter the identity of neocortical progenitors, leading to the failure to maintain a proper specification program in the developing neocortex.

Generation of interneurons derived from neocortical progenitors in the Sufu-cKO neocortex.

Given the widespread upregulation of ventral progenitor markers in neocortical progenitors, we wondered if this resulted in the production of neocortically-derived interneurons in the Sufu-cKO neocortex. We therefore examined Sufu-cKO mice carrying the conditional fluorescence reporter, ROSA26-AI14 (Madisen et al., 2010) (Sufu-cKO:AI14) to determine if interneurons were produced by Emx1-Cre -expressing (Emx1+) progenitors. At postnatal day (P) 12-14, we analyzed the identity of AI14-expressing (AI14+) cells in the neocortical grey matter of the control and Sufu-cKO:AI14 mice. Based on the expression of the pan-interneuron marker γ-aminobutyric acid (GABA+), we observed double-labeled cells in the P12 Sufu-cKO:AI14 neocortex whereas such double-labeled cells were less apparent in controls (**Figure 8A-8B, 8a'-b'**, yellow arrows). Quantification of double-labeled cells showed a 2-fold increase in those co-expressing AI14 and GABA in the P12

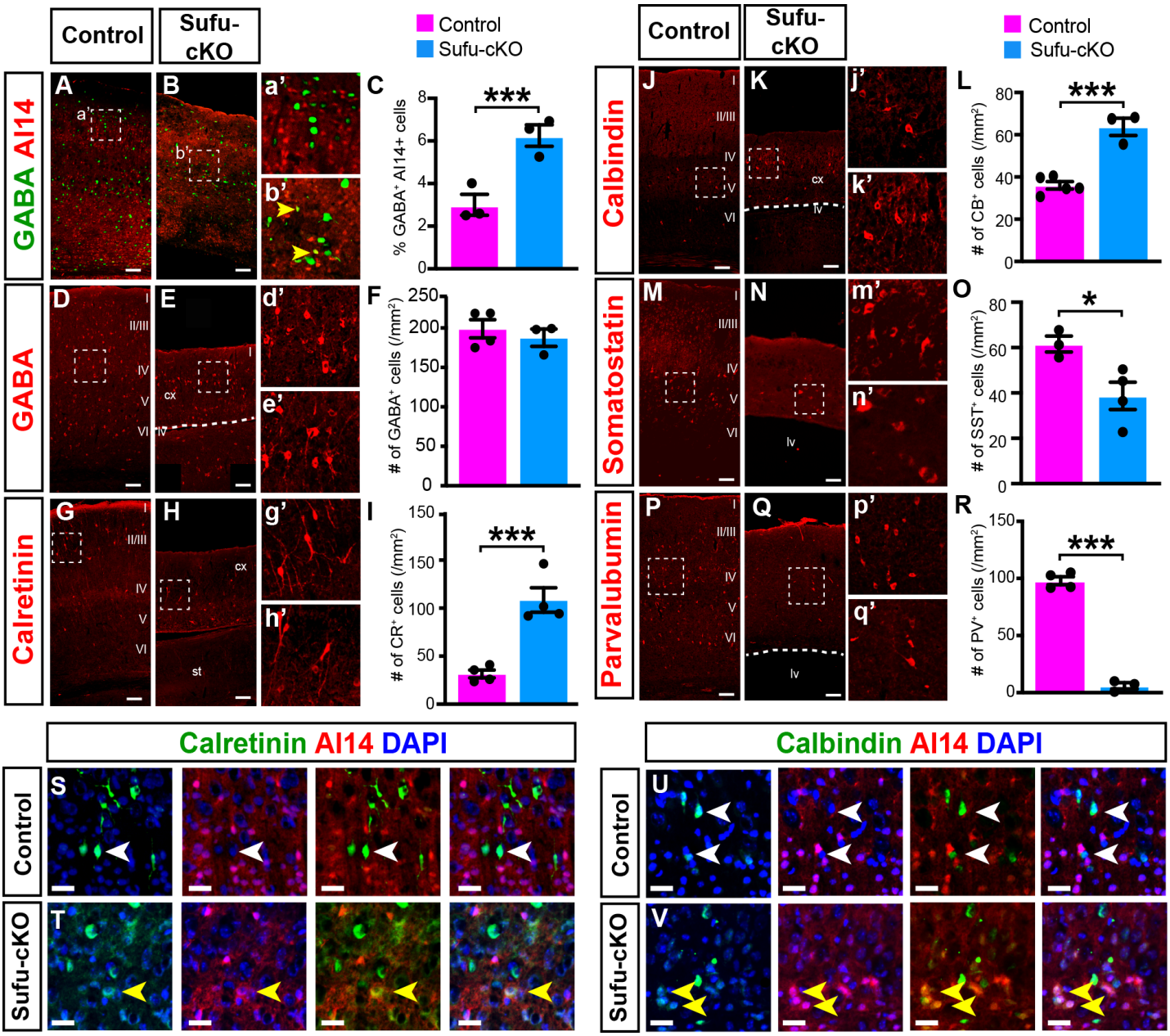

Figure 8. Sufu-cKO neocortical progenitors are capable of differentiating into specific interneuron subtypes.
A-C, Immunostaining against GABA on P12 control (A) and Sufu-cKO (B) neocortex carrying the ROSA26-Al14 transgene labeled neocortical-derived interneurons. Co-expression of Al14 (red) and GABA (green) are readily observed in Sufu-cKO neocortex (yellow arrows in b', higher magnification of boxed region in B) but not in controls (a', higher magnification of boxed region in A). Graph in C shows that a higher percentage of GABA+ cells are labeled with Al14 in the Sufu-cKO neocortex compared to controls. n = 3 mice/genotype (2-3 sections quantified). ***= p value ≤ 0.01.
D-F, Immunostaining against GABA show similar densities of GABA+ cells in the P14 control (D) and Sufu-cKO (E) neocortex. Dashed line in E represents the boundary between the neocortex (CX) and lateral ventricle (LV). GABA+ cells also display comparable neuronal morphology (d' and e' are higher magnification images of boxed region in D and E, respectively). Graph in F shows display equivalent GABA+ cell densities in the control and Sufu-cKO neocortex. n = 3-4 mice/genotype (2-3 sections quantified).
G-I, Immunostaining against the interneuron marker, Calretinin (CR) in the P14 control (G) and Sufu-cKO (H) neocortex. CR-expressing (CR+) cells are present in the control and Sufu-cKO P14 neocortex and exhibit a bipolar neuronal morphology (g' and h' are higher magnification images of boxed region in G and H, respectively). Quantification of the CR+ interneurons show higher density in the P14 Sufu-cKO neocortex compared to controls (I). n = 4 mice/genotype (2-3 sections quantified). ***= p value ≤ 0.01.
J-L, Immunostaining against the interneuron marker, Calbindin (CB) in the P14 control (J) and Sufu-cKO (K) neocortex. Dashed line in K represents the boundary between the neocortex (CX) and lateral ventricle (LV). CB-expressing (CB+) cells are present in the control and Sufu-cKO P14 neocortex and exhibit a neuronal morphology (j' and k' are higher magnification images of boxed region in J and K, respectively). Quantification of the CB+ interneurons show higher density in the P14 Sufu-cKO neocortex compared to controls (I). n =

Sufu-cKO neocortex over controls (**Figure 8C**). These findings indicated that loss of Sufu resulted in the generation of neocortical-derived GABAergic interneurons.

We previously showed no difference between the density of GABA+ cells in the P7 control and Sufu-cKO neocortex (Yabut et al., 2015). We therefore re-examined the density of GABAergic populations in the P12 neocortex to determine any changes between these two timepoints. Similar to our previous findings, we did not find obvious changes in GABA+ cell density between controls and Sufu-cKO neocortex (**Figure 8D-8F**). However, given the extensive diversity in interneuron subtypes, we examined four major subpopulations of GABAergic interneurons cells in the neocortex of control and Sufu-cKO mice according to subtype-specific markers: Calretinin (CR+), Calbindin (CB+), Somatostatin (SST+) or Parvalbumin (PV+) (Lim et al., 2018). We analyzed the distribution of these interneuron subtypes at P14, a timepoint at which expression of these interneuron markers are detectable in the neocortex. Indeed, all interneuron subtypes examined were present in the neocortex at this stage in both control and Sufu-cKO mice but exhibited differential densities. In particular, the density of CR+ and CB+ cells in the P14 Sufu-cKO neocortex were visibly increased (**Figure 8G-8H; 8J-8K**). Quantification of CR+ and CB+ cells showed ~2-3 -fold increase in the Sufu-cKO neocortex compared to controls (**Figure 8I, 8L**). In contrast, there were far fewer SST+ and PV+ cells detected in the Sufu-cKO neocortex (**Figure 8M-8N, 8P-8Q**). Quantification of SST+ and PV+ cells confirmed the significantly reduction in density in the Sufu-cKO neocortex compared to controls (**Figure 8N, 8Q**). Further examination of CR+ and CB+ cells in the P12 Sufu-cKO-AI14 showed that a small population of these cells also co-expressed AI14 (**Figure 8S-8V**). These findings suggest that some CR+ and CB+ interneurons were derived from neocortical progenitors. Taken together, our data indicate that loss of Sufu in early corticogenesis altered the fate and potential of neocortical progenitors leading to the ectopic production of interneurons.

DISCUSSION

Excitatory and inhibitory neurons in the mammalian neocortex are generated in a limited period of embryonic development and mature into molecularly diverse subpopulations at postnatal stages. A strict specification program is maintained by progenitors to generate precise numbers and neuronal lineages, relying on spatially and temporally modulated molecular cues present in neurogenic niches of the embryonic forebrain. Our study identified SHH and FGF15 signaling as key pathways that must be tightly modulated to ensure successful differentiation of neocortical progenitors into distinct excitatory neuron lineages in the course of corticogenesis. Further, we demonstrated that increasing SHH signaling can trigger differentiation of neocortical progenitors into interneurons. Therefore, our studies highlight the importance of Sufu as a key modulatory factor in establishing and maintaining neocortical progenitor programs.

Sufu regulates the stability and transcriptional activity of Gli transcription factors to control SHH signaling output particularly in neurogenic niches (Liu, 2019; Noguchi et al., 2019; Yin et al., 2019). In this study, we defined the molecular consequences of Sufu loss and the eventual degradation of Gli2 and Gli3 in the E12.5 neocortex (Yabut et al., 2015). Transcriptome profiles of neocortical progenitors were significantly altered in Sufu-cKO mice at E12.5, disrupting key molecular networks that maintain neuronal specification and differentiation programs. These changes pertained to the ectopic upregulation of SHH signaling target genes (e.g. Ptch1) and genes typically expressed in the GE (e.g. Olig2, Gsx2, Dlx1, Dbx2) in the E12.5 Sufu-cKO neocortex. Consistently, affected cells appeared in columnar patterns along the VZ/SVZ of the E12.5 Sufu-cKO neocortex, where abnormal progenitors were typically adjacent to each other and likely produced misspecified progenies that have radially migrated into the neocortical plate. Given the highly heterogeneous nature of the VZ/SVZ niche in the E12.5 neocortex (Telley et al., 2019), our findings strongly suggest that a subset of clonally-related RGCs are more vulnerable to molecular insults resulting from loss of

3-5 mice/genotype (2-3 sections quantified). ***= p value ≤ 0.01.

M-O, Immunostaining against the interneuron marker, Somatostatin (SST) in the P14 control (M) and Sufu-cKO (O) neocortex. SST-expressing (SST+) cells are present in the control and Sufu-cKO P14 neocortex (m' and o' are higher magnification images of boxed region in M and O, respectively). Quantification of the SST+ interneurons show lower density in the P14 Sufu-cKO **n**eocortex compared to controls (I). n = 3-4 mice/genotype (2-3 sections quantified). *= p value ≤ 0.05.

P-R, Immunostaining against the interneuron marker, Parvalbumin (PV) in the P14 control (P) and Sufu-cKO (Q) neocortex. Dashed line in Q represents the boundary between the neocortex (CX) and lateral ventricle (LV). PV-expressing (PV+) cells are present in the control and Sufu-cKO P14 neocortex (m' and o' are higher magnification images of boxed region in M and O, respectively). There are visibly much less PV+ cells in the P14 Sufu-cKO neocortex compared to controls. Graphs in R show significantly lower density of PV+ interneurons in the P14 Sufu-cKO neocortex. n = 4 mice/genotype (2-3 sections per animal was quantified). ***= p value ≤ 0.01.

S-T, Immunostaining against Calretinin (CR) on the neocortex of P14 mice carrying the ROSA26-AI14 transgene show neocortical-derived AI14+ cells labeled with CR in the Sufu-cKO neocortex (yellow arrow, T) but not in control neocortex (white arrow, S).

U-V, Immunostaining against Calbindin (CB) on the neocortex of P14 mice carrying the ROSA26-AI14 transgene show neocortical-derived AI14+ cells labeled with CB in the Sufu-cKO neocortex (yellow arrows, U) but not in control neocortex (white arrow, V).

Scale bars = 100 μm (A-Q) and 50 μm (S-V).

Sufu. Further supporting this, we found that the majority of progenitors in the rostral neocortical regions were specifically affected in the E12.5 Sufu-cKO neocortex. During normal corticogenesis, this region typically undergoes neuronal differentiation earlier than other regions of the neocortex (Takahashi et al., 1999) indicating that RGCs in this region are at a distinct differentiation stage. Likely, a subset of RGCs at this stage of neuronal differentiation have acquired unique transcriptional programs that strongly rely on Gli2 and/or Gli3 function, and that loss of Sufu derailed the developmental course of these progenitors.

Gli3R is the predominant isoform present in the developing neocortex and functions to control neural progenitor fates (Wang et al., 2011). It remained unclear, however, which genes are repressed by Gli3R to ensure normal progression of the neuronal specification program during corticogenesis. In this study, we found that the number of IPCs and their fates rely on low levels of FGF15. FGF15 is a known gene target of Gli3R, particularly at early stages of neural development for proper formation of telencephalic domains across the neuraxis (Kim et al., 2018; Rash and Grove, 2007; Wilson et al., 2012). In the developing neocortex, while FGF15 expression is very low, it plays important roles in the progression between progenitor proliferation and differentiation (Borello et al., 2008). However, the implications of high levels of FGF15 expression in the developing neocortex is largely unclear. Our studies show that increasing FGF15 gene expression, as a consequence of Sufu deletion and loss of Gli3R, resulted in very specific defects in the production and identity of neocortical IPCs. High levels of FGF15 activated FGF signaling in turn triggered the activation of MAPK signaling. Interestingly, we observed ectopic activation of MAPK signaling specifically in the VZ/SVZ by E13.5 in the developing neocortex of Sufu-cKO mice. These findings indicate that neocortical progenitors, particularly RGCs, are especially vulnerable to variations in FGF signals, and must be attenuated to ensure proper maintenance of the specification program.

Expansion of upper layer excitatory neurons, which drives gyrification of the cerebral cortex in several mammalian species including humans, has been attributed to the increase in SHH signaling activity during corticogenesis (Kang et al., 2011; Miller et al., 2014; Molnár et al., 2006; Wang et al., 2016). Coincidentally, interneuron differentiation from a subset of neocortical progenitors has also been reported in fetal primate neocortex in a number of studies (Alzu'bi and Clowry, 2019; Radonjić et al., 2014; Yu and Zecevic, 2011). Whether interneuron production from neocortical progenitors is due to the increase in SHH signaling activity in primates is yet to be examined. However, our studies strongly support this possibility given the induction of ventral forebrain progenitor gene expression in the E12.5 Sufu-cKO neocortex, and the eventual generation of neocortical-derived interneurons. The differential densities of interneuron subtypes suggest a preferential production and survival of CR+ and CB+ interneurons from neocortical progenitors. However, we cannot exclude the possibility that the decrease in PV+ or SST+ was due to delayed differentiation, cell death, or the failure of GE-derived interneurons to properly migrate into the neocortex given the severe neocortical defects. Nevertheless, that we observed CR+ and CB+ cells co-expressing Emx1-driven AI14 expression, strongly indicate that Sufu-cKO neocortical progenitors have gained the capacity to differentiate into interneurons. Clearly, activation of SHH signaling at early stages of corticogenesis, and consequently with activated FGF and MAPK signaling, can profoundly alter the molecular landscape and the fate potential of neocortical progenitors and their progenies. It remains to be determined how the combinatorial action of these pathways direct the production of specific neuronal subtypes in the neocortex to result in the evolutionary expansion and functional complexity of the cerebral cortex in humans.

Along with the expansion and diversification of neocortical neuron subtypes in the human brain, anomalies in the number, differentiation, and maturation of upper layer excitatory neurons and interneurons are now known to underlie a number of neuropsychiatric and neurodevelopmental disorders. The activation of FGF and MAPK signaling cascades, in response to SHH signaling activation, indicate important potential implications of uncontrolled SHH signaling in these disorders. For instance, it is evident that abnormal numbers and specification of neuronal subtypes lead to aberrant circuits in autism spectrum disorders (ASD) (Kaushik and Zarbalis, 2016). High serum levels of SHH and deregulated FGF signaling activity at developmental stages has been implicated in these defects (Al-Ayadhi, 2012; Halepoto et al., 2015; Rubenstein, 2011; Vaccarino et al., 2009). Thus, further investigation of how pathogenic SHH and FGF signaling converge to produce abnormal neuronal subtypes, and drive abnormal neocortical circuitry, could lay the foundation towards detecting, treating, or even reversing the neocortical abnormalities present in neurodevelopmental disorders.

EXPERIMENTAL PROCEDURES

Animals:

Mice carrying the floxed Sufu allele (Sufufl) were kindly provided by Dr. Chi-Chung Hui (University of Toronto) and were genotyped as described elsewhere (Pospisilik et al., 2010). Emx1-cre (Stock #05628), Rosa-AI14 (Stock #007908), SmoM2 (Stock #005130) mice were obtained from Jackson Laboratories (Bar Harbor, ME, USA). Mice

designated as controls did not carry the Cre transgene and may have either one of the following genotypes: Sufufl/+ or Sufufl/fl. All mouse lines were maintained in mixed strains, and analysis included male and female pups from each age group, although sex differences were not included in data reporting. All animal protocols were in accordance to the National Institute of Health regulations and approved by the UCSF Institutional Animal Care and Use Committee (IACUC).

RNA-Seq and Analysis:

The dorsal forebrain was dissected from E12.5 control and Sufu-cKO littermates (n=4 per group). Total RNA was extracted using Qiagen RNEasy Mini Kit (Qiagen) and prepared for RNAseq. RNASeq was conducted by the UCSF Functional Genomics Core. Barcoded sequencing libraries were generated using the Truseq Stranded mRNA Library Prep Kit (Illumina). Single-end 50-bp reads were sequenced on the HiSeq4000 (Illumina). Sequencing yielded ~343 million read with an average read depth of 42.9 million reads/sample. Reads were then aligned using STAR_2.4.2a to the mouse genome (Ensembl Mouse GRCm38.78) and those that mapped uniquely to known mRNAs were used to assess differential expression (DE). Final quantification and statistical testing of differentially expressed (adjusted $P < 0.05$) genes were performed using DESeq2. Gene set enrichment and pathway analysis was conducted using The DAVID Gene Functional Classification Tool http://david.abcc.ncifcrf.gov (Huang et al., 2007). Heatmaps represent transformed FPKM values (Transform 1+ Log2(Y)) and plotted using Prism 8.1 (GraphPad). Filtering was applied for GO enrichment analysis by excluding DE genes with very low normalized read counts (FPKM <100) in both control and mutant samples.

Immunohistochemistry:

Perfusion, dissection, and immunofluorescence staining were conducted according to standard protocols as previously described (Siegenthaler et al., 2009). Briefly, embryonic brain tissues were fixed by direct immersion in 4% paraformaldehyde (PFA) and postnatal brains fixed by intracardial perfusion followed by 2 h post-fixation. Cryostat sections were air dried and rinsed 3× in PBS plus 0.2%Triton before blocking for 1 h in 10% normal lamb serum diluted in PBS with 0.2% Triton to prevent nonspecific binding. A heat-induced antigen retrieval protocol was performed on selective immunohistochemistry using 10 □M Citric Acid at pH 6.0. Primary antibodies were diluted in 10% serum diluted in PBS with 0.2% Triton containing 40,6-diamidino-2-phenylindole (DAPI); sections were incubated in primary antibody overnight at room temperature. The following antibodies were used: rabbit anti-Tbr2 (1:500 dilution; Abcam (#ab23345), Cambridge, UK), rabbit anti-GSX2 (1:250 dilution; gift from Kenneth Campbell (Toresson et al., 2000)) mouse anti-Olig2 (1:250 dilution; Millipore (#MABN50), Billerica, MA, USA), rabbit anti-GABA (1:500; Sigma A2052), mouse anti-calretinin (1:250; Millipore MAB1568), rabbit anti-calbindin (1:500; Swant CB-28a), rat anti-somatostatin (1:100; Millipore MAB354), mouse anti-parvalbumin (1:500; Millipore MAB1572). To detect primary antibodies, we used species-specific Alexa Fluor-conjugated secondary antibodies (1:500; Invitrogen) in 1X PBS-T for 1 h at room temperature, washed with 1X PBS, and coverslipped with Fluoromount-G (SouthernBiotech).

In Situ Hybridization:

Lhx2, CoupTF2 in situ hybridization (ISH) was conducted using RNA probes kindly provided by Professor John Rubenstein (University of California San Francisco). Dlx1 and Dbx1 riboprobles were generated using primer sequences published by the Allen Brain Atlas ISH Database (http://developingmouse.brain-map.org/) with SP6 and T7 promoter binding sequences included in 5' ends. Target gene cDNA was amplified from pooled cDNA reactions made from mouse brain total RNA were used as a template source. DIG-labeled RNA probes were generated using the DIG RNA Labeling Kit SP6/T7 (Sigma-Aldrich cat. # 11175025910) according to manufacturer's protocols. DIG-labeled RNA probes were diluted in hybridization buffer (50% formamide, 5 x SSC, 0.3 mg/ml tRNA, 100 µl/ml Heparin, 1x Denhardt's solution, 0.1% Tween 20, 0.1% CHAPS, 5 mM EDTA) and added to RNase-free cryosections for incubation in a humidified chamber at 65°C for 16-20h. Sections were washed in 0.2 x SSC (Ambion AM9770) at 65°C followed by PBST at room temperature. Tissue sections were incubated in alkaline phosphatase-conjugated anti-DIG antibody (1:1500, Roche Applied Sciences 11093274910) for 16-20h incubation at room temperature and colorimetric signals were detected using Nitro blue tetrazolium chloride and 5-bromo-4-chloro-3-indolyl phosphase (NBT-BCIP; Roche Applied Sciences 11383221001).

RNAScope ISH was conducted for FGF15 and Ptch1. RNAscope probes Mm-Ptch1 (Cat No. 402811) and Mm-FGF15 (Cat No. 412811) were designed commercially by the manufacturer (Advanced Cell Diagnostics, Inc.). RNAScope Assay was performed using the RNAscope Multiplex Fluorescent Reagent Kit V2 according to manufacturer's instructions. Detection of the probe was done with Opal 570 or Opal 520 reagent (Perkin Elmer).

Forebrain Organotypic Slice Culture:

Whole brains from E12.5 wildtype CD-1 mice were carefully dissected and placed in ice-cold Hanks Balanced Salt Solution (HBSS; Invitrogen). Brains were embedded in 4% Low Melting Point Agarose (Nueve)/HBSS mix and allowed to solidify on ice. Embedded brains were sliced using a VT1000S vibratome (Leica) into 400 □m thick slices and placed in Recovery Media (MEM (Invitrogen) with Glutamax (Invitrogen) and Pennicillin/Streptomycin (Invitrogen)). Slices were transferred into uncoated Millicell-CM membrane inserts (EMD-Millipore) in 6-well plates (BD Biosciences) and cultured in Neurobasal (Invitrogen) supplemented with

Glutamax (Invitrogen), Pennicillin/Streptomycin (Invitrogen), B-27 (Invitrogen) and N2 (Invitrogen) at 37°C, 5% CO2, and 100% humidity. After 2 days in vitro (DIV), cell culture media were aspirated, and slices were washed in 1X PBS, fixed in cold 4% PFA for 30 minutes, cryoprotected in 30% sucrose, and embedded in OCT. Slices were cryosectioned into 20 m thick coronal sections and stored at -80°C until used for immunofluorescence analysis as described above. Treatment (as described in text) of organotypic slices were conducted 2-3 hours after initial plating and incubation of slices with the following concentrations: 100 ng/ml recombinant FGF15 (Prospec Bio, #CYT-027), 200 ng/ml recombinant SHH (GenScript, #Z03050-50), and 5 uM cyclopamine (Toronto Research Chemicals, #C988400). Following treatments, slice cultures were incubated for 2 days and processed as described above.

Image Analysis and Acquisition:

Images were acquired using a Nikon E600 microscope equipped with a QCapture Pro camera (QImaging), Zeiss Axioscan Z.1 (Zeiss, Thornwood, NY, USA) using the Zen 2 blue edition software (Zeiss, Thornwood, NY, USA), or the Nikon Ti inverted microscope with CSU-W1 large field of view confocal and Andor Zyla 4.2 sCMOS camera. NIH Image J was used to quantify raw, unedited images. All analyses were conducted in at least 2-3 20 m thick sections that were histologically matched at the rostral-caudal level between genotypes.

Statistics:

All experiments were conducted in triplicate with a sample size of n = 3−6 embryos/animals per genotype. Unpaired Student t-test was conducted using Prism 8.1 (GraphPad) for pairwise analysis of control and mutant genotypes. P value ≤0.05 were considered statistically significant. Graphs display the mean ± standard error of the mean (SEM).

ACKNOWLEDGMENTS

We would like to thank members of the Pleasure Lab for helpful discussions, Dr. Kenneth Campbell for the Gsx2 antibody, and DeLaine Larsen and Kari Harrington at the University of California San Francisco Nikon Imaging Center for assistance with imaging. This work was supported by the NIH R01 NS075188 (S.J.P.), NIH/NCI K01CA201068 (O.R.Y.), KNRF 2019M3A9H1103702 (KY), and NIH/NINDS R01MH077694-S1 (H.G.).

COMPETING INTERESTS

The authors declare no competing or financial interests.

REFERENCES

Al-Ayadhi LY. 2012. Relationship Between Sonic Hedgehog Protein, Brain-Derived Neurotrophic Factor and Oxidative Stress in Autism Spectrum Disorders. Neurochem Res 37:394–400. doi:10.1007/s11064-011-0624-x

Alzu'bi A, Clowry GJ. 2019. Expression of ventral telencephalon transcription factors ASCL1 and DLX2 in the early fetal human cerebral cortex. J Anat 235:555–568. doi:10.1111/joa.12971

Beattie R, Hippenmeyer S. 2017. Mechanisms of radial glia progenitor cell lineage progression. FEBS Lett 591:3993–4008. doi:10.1002/1873-3468.12906

Borello U, Cobos I, Long JE, Murre C, Rubenstein JL. 2008. FGF15 promotes neurogenesis and opposes FGF8 function during neocortical development. Neural Dev 3:17. doi:10.1186/1749-8104-3-17

Dave RK, Ellis T, Toumpas MC, Robson JP, Julian E, Adolphe C, Bartlett PF, Cooper HM, Reynolds BA, Wainwright BJ. 2011. Sonic hedgehog and notch signaling can cooperate to regulate neurogenic divisions of neocortical progenitors. PLoS One 6:e14680. doi:10.1371/journal.pone.0014680

Fotaki V, Yu T, Zaki PA, Mason JO, Price DJ. 2006. Abnormal positioning of diencephalic cell types in neocortical tissue in the dorsal telencephalon of mice lacking functional Gli3. J Neurosci 26:9282–92. doi:10.1523/JNEUROSCI.2673-06.2006

Gimeno L, Martinez S. 2007. Expression of chickFgf19 and mouseFgf15 orthologs is regulated in the developing brain byFgf8 andShh. Dev Dyn 236:2285–2297. doi:10.1002/dvdy.21237

Guillemot F, Zimmer C. 2011. From Cradle to Grave: The Multiple Roles of Fibroblast Growth Factors in Neural Development. Neuron 71:574–588. doi:10.1016/J.NEURON.2011.08.002

Halepoto DM, Bashir S, Zeina R, Al-Ayadhi LY. 2015. Correlation Between Hedgehog (Hh) Protein Family and Brain-Derived Neurotrophic Factor (BDNF) in Autism Spectrum Disorder (ASD). J Coll Physicians Surg Pak 25:882–5. doi:12.2015/JCPSP.882885

Hevner RF. 2019. Intermediate progenitors and Tbr2 in cortical development. J Anat 235:616–625. doi:10.1111/joa.12939

Huang DW, Sherman BT, Tan Q, Collins JR, Alvord WG, Roayaei J, Stephens R, Baseler MW, Lane HC, Lempicki RA. 2007. The DAVID Gene Functional Classification Tool: a novel biological module-centric algorithm to functionally analyze large gene lists. Genome Biol 8:R183. doi:10.1186/gb-2007-8-9-r183

Kang HJ, Kawasawa YI, Cheng F, Zhu Y, Xu X, Li M, Sousa AMM, Pletikos M, Meyer KA, Sedmak G, Guennel T, Shin Y, Johnson MB, Krsnik Ž, Mayer S, Fertuzinhos S, Umlauf S, Lisgo SN, Vortmeyer A, Weinberger DR, Mane S, Hyde TM, Huttner A, Reimers M, Kleinman JE, Šestan N. 2011. Spatio-temporal transcriptome of the human brain. Nature 478:483–489. doi:10.1038/nature10523

Kaushik G, Zarbalis KS. 2016. Prenatal Neurogenesis in Autism Spectrum Disorders. Front Chem 4:12. doi:10.3389/fchem.2016.00012

Kim JJ, Jiwani T, Erwood S, Loree J, Rosenblum ND. 2018. Suppressor of fused controls cerebellar neuronal differentiation in a manner modulated by GLI3 repressor and Fgf15. Dev Dyn 247:156–169. doi:10.1002/dvdy.24526

Komada M, Saitsu H, Kinboshi M, Miura T, Shiota K, Ishibashi M. 2008a. Hedgehog signaling is involved in development of the neocortex. Development 135:2717–27. doi:10.1242/dev.015891

Komada M, Saitsu H, Shiota K, Ishibashi M. 2008b. Expression of Fgf15 is regulated by both activator and repressor forms of Gli2 in vitro. Biochem Biophys Res Commun 369:350–356. doi:10.1016/J.BBRC.2008.02.015

Lim L, Mi D, Llorca A, Marín O. 2018. Development and Functional Diversification of Cortical Interneurons. Neuron 100:294–313. doi:10.1016/J.NEURON.2018.10.009

Liu A. 2019. Proteostasis in the Hedgehog signaling pathway. Semin Cell Dev Biol 93:153–163. doi:10.1016/j.semcdb.2018.10.009

Long F, Zhang XM, Karp S, Yang Y, McMahon AP. 2001. Genetic manipulation of hedgehog signaling in the endochondral skeleton reveals a direct role in the regulation of chondrocyte proliferation. Development 128:5099–5108.

Madisen L, Zwingman TA, Sunkin SM, Oh SW, Zariwala HA, Gu H, Ng LL, Palmiter RD, Hawrylycz MJ, Jones AR, Lein ES, Zeng H. 2010. A robust and high-throughput Cre reporting and characterization system for the whole mouse brain. Nat Neurosci 13:133–40. doi:10.1038/nn.2467

Miller JA, et al. 2014. Transcriptional landscape of the prenatal human brain. Nature 508:199–206. doi:10.1038/nature13185

Miyoshi G, Butt SJB, Takebayashi H, Fishell G. 2007. Physiologically distinct temporal cohorts of cortical interneurons arise from telencephalic Olig2-expressing precursors. J Neurosci 27:7786–98. doi:10.1523/JNEUROSCI.1807-07.2007

Molnár Z, Métin C, Stoykova A, Tarabykin V, Price DJ, Francis F, Meyer G, Dehay C, Kennedy H. 2006. Comparative aspects of cerebral cortical development. Eur J Neurosci 23:921–934. doi:10.1111/j.1460-9568.2006.04611.x

Noguchi H, Castillo JG, Nakashima K, Pleasure SJ. 2019. Suppressor of fused controls perinatal expansion and quiescence of future dentate adult neural stem cells. Elife 8. doi:10.7554/eLife.42918

Palma V, Ruiz i Altaba A. 2004. Hedgehog-GLI signaling regulates the behavior of cells with stem cell properties in the developing neocortex. Development 131:337–45. doi:10.1242/dev.00930

Petryniak MA, Potter GB, Rowitch DH, Rubenstein JLR. 2007. Dlx1 and Dlx2 control neuronal versus oligodendroglial cell fate acquisition in the developing forebrain. Neuron 55:417–33. doi:10.1016/j.neuron.2007.06.036

Radonjić NV, Ayoub AE, Memi F, Yu X, Maroof A, Jakovcevski I, Anderson SA, Rakic P, Zecevic N. 2014. Diversity of Cortical Interneurons in Primates: The Role of the Dorsal Proliferative Niche. Cell Rep 9:2139–2151. doi:10.1016/j.celrep.2014.11.026

Rash BG, Grove EA. 2007. Patterning the dorsal telencephalon: a role for sonic hedgehog? J Neurosci 27:11595–603. doi:10.1523/JNEUROSCI.3204-07.2007

Rubenstein JLR. 2011. Annual Research Review: Development of the cerebral cortex: implications for neurodevelopmental disorders. J Child Psychol Psychiatry 52:339–355. doi:10.1111/j.1469-7610.2010.02307.x

Siegenthaler JA, Ashique AM, Zarbalis K, Patterson KP, Hecht JH, Kane MA, Folias AE, Choe Y, May SR, Kume T, Napoli JL, Peterson AS, Pleasure SJ. 2009. Retinoic acid from the meninges regulates cortical neuron generation. Cell 139:597–609. doi:10.1016/j.cell.2009.10.004

Sohal VS, Rubenstein JLR. 2019. Excitation-inhibition balance as a framework for investigating mechanisms in neuropsychiatric disorders. Mol Psychiatry 24:1248–1257. doi:10.1038/s41380-019-0426-0

Takahashi T, Goto T, Miyama S, Nowakowski RS, Caviness VS. 1999. Sequence of neuron origin and neocortical laminar fate: relation to cell cycle of origin in the developing murine cerebral wall. J Neurosci 19:10357–71. doi:10.1523/JNEUROSCI.19-23-10357.1999

Telley L, Agirman G, Prados J, Amberg N, Fièvre S, Oberst P, Bartolini G, Vitali I, Cadilhac C, Hippenmeyer S, Nguyen L, Dayer A, Jabaudon D. 2019. Temporal patterning of apical progenitors and their daughter neurons in the developing neocortex. Science 364:eaav2522. doi:10.1126/science.aav2522

Toresson H, Potter SS, Campbell K. 2000. Genetic control of dorsal-ventral identity in the telencephalon: opposing roles for Pax6 and Gsh2. Development 127:4361–71.

Vaccarino FM, Grigorenko EL, Smith KM, Stevens HE. 2009. Regulation of Cerebral Cortical Size and Neuron Number by Fibroblast Growth Factors: Implications for Autism. J Autism Dev Disord 39:511–520. doi:10.1007/s10803-008-0653-8

Wang H, Ge G, Uchida Y, Luu B, Ahn S. 2011. Gli3 is required for maintenance and fate specification of cortical progenitors. J Neurosci 31:6440–8. doi:10.1523/JNEUROSCI.4892-10.2011

Wang L, Hou S, Han Y-G. 2016. Hedgehog signaling promotes basal progenitor expansion and the growth and folding of the neocortex. Nat Neurosci. doi:10.1038/nn.4307

Wang Y, Kim E, Wang X, Novitch BG, Yoshikawa K, Chang L-S, Zhu Y. 2012. ERK Inhibition Rescues Defects in Fate Specification of Nf1-Deficient Neural Progenitors and Brain Abnormalities. Cell 150:816–830. doi:10.1016/j.cell.2012.06.034

Wilson SL, Wilson JP, Wang C, Wang B, McConnell SK. 2012. Primary cilia and Gli3 activity regulate cerebral cortical size. Dev Neurobiol 72:1196–212. doi:10.1002/dneu.20985

Yabut OR, Fernandez G, Huynh T, Yoon K, Pleasure SJSJ. 2015. Suppressor of Fused Is Critical for Maintenance of Neuronal Progenitor Identity during Corticogenesis. Cell Rep 12:2021–34. doi:10.1016/j.celrep.2015.08.031

Yin W-C, Satkunendran T, Mo R, Morrissy S, Zhang X, Huang ES, Uusküla-Reimand L, Hou H, Son JE, Liu W, Liu YC, Zhang J, Parker J, Wang X, Farooq H, Selvadurai H, Chen X, Sau-Wai Ngan E, Cheng SY, Dirks PB, Angers S, Wilson MD, Taylor MD, Hui C. 2019. Dual Regulatory Functions of SUFU and Targetome of GLI2 in SHH Subgroup Medulloblastoma. Dev Cell 48:167-183.e5. doi:10.1016/j.devcel.2018.11.015

Ypsilanti AR, Rubenstein JLR. 2016. Transcriptional and epigenetic mechanisms of early cortical development: An examination of how Pax6 coordinates cortical development. J Comp Neurol 524:609–629. doi:10.1002/cne.23866

Yu X, Zecevic N. 2011. Dorsal Radial Glial Cells Have the Potential to Generate Cortical Interneurons in Human But Not in Mouse Brain. J Neurosci 31:2413–2420. doi:10.1523/JNEUROSCI.5249-10.2011

Supplemental Table 1: Expression of select genes typically expressed by dorsal or ventral progenitors in individual control and Sufu-cKO mice (n=4 mice per genotype).

	Ensembl_ID	Gene	MutvsCont. FC	Mutvs-Cont. log2FC	MutvsCont. RawP	MutvsCont. FDR	Control #1	Control #2	Control #3	Control #4	Mutant #1	Mutant #2	Mutant #3	Mutant #4
Dorsal Forebrain Progenitor Specific Genes	ENSMUSG00000027168	Pax6	1.45	0.54	1.00E-08	7.70E-07	7490.66	7888.50	6561.05	7396.29	10797.78	10922.72	9795.55	11074.18
	ENSMUSG00000035033	Tbr1	1.23	0.29	0.002157282	0.039548605	6740.01	6917.21	7112.83	7369.47	7974.87	8744.25	8446.03	9306.47
	ENSMUSG00000032446	Eomes	1.09	0.13	0.15380485	0.798831638	8713.63	9479.93	9457.86	7463.78	8975.79	10324.15	8920.21	10217.53
	ENSMUSG00000033726	Emx1	0.60	-0.73	3.25E-06	0.000146525	1343.15	1747.87	1721.38	1540.17	1218.38	984.60	897.88	738.94
	ENSMUSG00000043969	Emx2	0.61	-0.72	1.18E-13	2.02E-11	6614.55	6507.54	5290.42	6266.25	3705.96	4122.72	3659.13	3489.93
	ENSMUSG00000048562	Sp8	0.54	-0.90	0.000188789	0.005208489	1801.76	1364.08	1079.26	1505.56	989.75	555.19	660.79	886.33
	ENSMUSG00000000247	Lhx2	0.70	-0.51	6.80E-08	4.42E-06	16465.75	19498.97	18322.18	16670.20	13435.74	13745.30	10924.21	11699.36
	ENSMUSG00000069171	Nr2f1	1.59	0.67	0.000146447	0.004158221	5948.25	7115.30	7966.72	7656.73	9186.14	13954.58	11875.28	10611.23
	ENSMUSG00000030551	Nr2f2	2.63	1.39	0.000483548	0.011540833	1123.86	975.79	1501.83	1322.99	1876.86	3988.26	4415.48	2657.01
Ventral Forebrain Progenitor Specific Genes	ENSMUSG00000001496	Nkx2-1	0.22	-2.17	0.399106005	1	5.27	0	93.26	2.60	14.23	0	7.21	0.99
	ENSMUSG00000044220	Nkx2-3	10.15	3.34	7.38E-20	2.12E-17	41.12	25.89	31.09	40.67	430.85	235.31	338.96	402.61
	ENSMUSG00000030507	Dbx1	38.02	5.25	3.63E-26	2.09E-23	42.17	10.13	30.11	28.55	1496.81	887.00	841.99	993.16
	ENSMUSG00000045608	Dbx2	47.19	5.56	3.73E-43	4.49E-40	2.11	4.50	0	6.92	128.04	147.47	202.83	160.25
	ENSMUSG00000046160	Olig1	9.36	3.23	4.66E-09	3.90E-07	8.43	5.63	3.89	6.92	78.24	28.19	64.01	62.32
	ENSMUSG00000039830	Olig2	12.61	3.66	2.65E-10	2.70E-08	87.51	42.77	77.71	70.09	1101.52	404.46	869.93	1130.66
	ENSMUSG00000045591	Olig3	7.20	2.85	8.34E-12	1.07E-09	10.54	2.25	3.89	4.33	37.60	32.53	39.67	41.55
	ENSMUSG00000053129	Gsx1	1.36	0.44	0.856429159	1	0	0	8.74	0	6.10	0	1.80	3.96
	ENSMUSG00000035946	Gsx2	9.20	3.20	8.71E-05	0.002714615	22.14	3.38	20.40	117.68	522.31	112.77	334.45	535.16
	ENSMUSG00000041911	Dlx1	3.10	1.63	0.079709861	0.569816271	204.53	52.90	396.34	1190.61	2300.60	276.51	1017.78	2120.86
	ENSMUSG00000023391	Dlx2	3.95	1.98	0.023529515	0.251170124	72.75	32.64	159.31	475.03	1070.02	155.06	581.46	1115.83
	ENSMUSG00000020052	Ascl1	1.72	0.79	0.001077842	0.02236943	1250.38	1109.73	1435.78	1528.92	2609.51	1495.33	2324.93	2748.02

Supplemental Table 2: Top differentially expressed genes encoding extracellular matrix or cell membrane bound proteins between control and Sufu-cKO mice (n=4 mice per genotype)

Gene	Mutvs-Cont.FC	Mutvs-Cont. log2FC	Mutvs-Cont. RawP	Mutvs-Cont. FDR	Control #1	Control #2	Control #3	Control #4	Mutant #1	Mutant #2	Mutant #3	Mutant #4	Control_ AVG	Mutant_ Avg
Hhip	82.08	6.36	6.07E-54	9.03E-51	12.65	5.63	8.74	8.65	579.21	618.08	845.59	885.34	8.92	732.06
Fgf15	52.70	5.72	1.38E-96	1.16E-92	223.51	72.03	42.74	270.83	8031.77	6354.33	8400.95	9315.37	152.28	8025.61
Fgf15	52.70	5.72	1.38E-96	1.16E-92	223.51	72.03	42.74	270.83	8031.77	6354.33	8400.95	9315.37	152.28	8025.61
Spon1	14.95	3.90	2.55E-158	3.23E-154	34.79	60.78	42.74	86.53	911.50	805.68	764.46	880.40	56.21	840.51
Ptch1	10.50	3.39	5.01E-57	8.45E-54	600.94	625.77	682.92	860.94	6527.85	6328.30	7650.01	8592.26	692.64	7274.61
Lypd6	6.23	2.64	3.73E-23	1.55E-20	648.38	607.76	889.83	712.98	3218.20	5292.74	4715.68	4593.88	714.74	4455.12
Lypd1	5.78	2.53	1.68E-14	3.08E-12	108.59	95.67	123.37	105.56	789.56	533.50	458.86	722.12	108.30	626.01
Pdgfa	5.61	2.49	8.41E-17	1.95E-14	181.34	183.45	219.54	269.10	1060.88	1541.95	1258.48	925.90	213.36	1196.80
Adamts20	5.09	2.35	8.48E-35	7.66E-32	865.56	702.30	871.37	1077.26	3917.32	5338.28	4605.69	4054.76	879.12	4479.02
Smoc1	3.28	1.71	5.24E-06	0.000224706	168.68	136.18	202.06	275.15	749.93	342.66	745.53	728.06	195.52	641.54
Adamts19	0.26	-1.95	3.80E-07	2.12E-05	707.42	450.19	534.29	330.53	109.75	124.70	146.94	143.44	505.61	131.21
Vcam1	0.26	-1.97	8.06E-61	2.04E-57	2910.87	3106.33	3090.13	2571.57	686.93	580.13	916.81	798.29	2919.72	745.54
Bcan	0.07	-3.93	2.64E-13	4.31E-11	527.14	557.11	443.94	225.83	45.73	21.69	7.21	40.56	438.51	28.80